# Multi-Objective Optimization of Hybrid Heat Sinks with Phase Change Materials

Nedumaran, Muthamil Selvan; Trilok, Govindappa; Gnanasekaran, Nagarajan; Hooman, Kamel

**DOI**
10.1080/01457632.2023.2234770

**Publication date**
2023

**Document Version**
Final published version

**Published in**
Heat Transfer Engineering

**Citation (APA)**
Nedumaran, M. S., Trilok, G., Gnanasekaran, N., & Hooman, K. (2023). Multi-Objective Optimization of Hybrid Heat Sinks with Phase Change Materials. *Heat Transfer Engineering*, *45 (2024)*(11), 1028-1049. https://doi.org/10.1080/01457632.2023.2234770

Heat Transfer Engineering

ISSN: (Print) (Online) Journal homepage: https://www.tandfonline.com/loi/uhte20

# Multi-Objective Optimization of Hybrid Heat Sinks with Phase Change Materials

Muthamil Selvan Nedumaran, Govindappa Trilok, Nagarajan Gnanasekaran & Kamel Hooman

**To cite this article:** Muthamil Selvan Nedumaran, Govindappa Trilok, Nagarajan Gnanasekaran & Kamel Hooman (2023): Multi-Objective Optimization of Hybrid Heat Sinks with Phase Change Materials, Heat Transfer Engineering, DOI: 10.1080/01457632.2023.2234770

**To link to this article:** https://doi.org/10.1080/01457632.2023.2234770

Published online: 17 Jul 2023.

HEAT TRANSFER ENGINEERING
https://doi.org/10.1080/01457632.2023.2234770

Taylor & Francis
Taylor & Francis Group



# Multi-Objective Optimization of Hybrid Heat Sinks with Phase Change Materials

Muthamil Selvan Nedumaran[a], Govindappa Trilok[a], Nagarajan Gnanasekaran[a], and Kamel Hooman[b]

[a]Department of Mechanical Engineering, National Institute of Technology Karnataka, Surathkal, India; [b]Department of Process and Energy, Delft University of Technology, Delft, Netherlands

**ABSTRACT**

A passive method with phase change material (PCM) is an appropriate technique in electronic cooling. But, due to its poor thermal conductivity, many enhancers are employed to reduce the thermal resistance offered by the PCM. A partial filling strategy to reduce the cost and weight of foams with fins is used in this study. A hybrid heat sink with a combination of fins placed at the sidewalls of the enclosure and foams filled at certain heights such as 10, 20, and 30 mm is considered in this present work. A two-dimensional numerical model with n-eicosane as PCM is developed in ANSYS Fluent 19. A multi-objective optimization is carried out using a reliable multi criteria decision making approach. Different weightage is distributed to the objective functions in this method depending on the choice of the user. The pore size and density vary for various filling heights, and 60 cases are investigated for both charging and discharging cycles. The pore size of 0.8-0.95 and pore density of 5-25 pores per inch with a broad range is considered. From the discussions, guidelines for selecting a preferable pore size and pore density can be determined based on the filling height and applied weightage.

## Introduction

The miniaturization of electronic devices has increased thermal stress, making compact cooling techniques essential. Conventional heat sinks provide the desired compactness to operate the devices under safety limits. Heat sinks absorb heat from the devices and dissipate heat to the surrounding so that the reliability of the device is enhanced. A passive type of heat sink is filled with phase change material (PCM). PCM by phase conversion can store heat energy. When the PCM absorbs the heat, it converts from a solid to a liquid state. When the heat is extracted from the PCM, it reforms to a solid state. PCM has numerous advantages, but the major drawback is poor thermal conductivity. This high resistance can be overcome by adding some enhancers and these enhancers increase the heat flow within the sink. Several enhancers like fins [1–5], foams [6–10], nano additives [11–15], and heat pipes [16–18] have been used in recent years.

Desai et al. [19] introduced inverted fin geometry to control the electronic device power surges. The shape of the fin structures is also varied along with fin numbers. The shapes considered are triangular prism, star prism, triangular frustum, and star frustum. The star inverted fin structure provides exceptional performance. The surface area increases and the melting rate of PCM also enhances by increasing the fin number. The effect of adding combined fractal fins to the shell and tube heat exchanger was studied by Luo et al. [20]. The combined fractal fins provide a uniform temperature distribution within PCM. The melting cycle was analyzed by obtaining an expression for the thermal response coefficient and uniform temperature distribution. Singh and Giri [21] experimentally developed a dual height pin fin for electronic cooling. The number of pin fins, type of fins, and fin volume fraction vary for different heat flux ranges. The results indicate that 40 dual height pin fins and 9% volume fraction enhanced output. Chen et al. [22] explored the melting behavior of PCM when immersed with metal foams. Adding foams to the PCM, natural convection weakens while conduction becomes dominant. Furthermore, the structure of metal foam significantly affects the melting. High alcohol/high graphite foam integrated PCM-based heat sink was presented by Wang et al. [23]. The

CONTACT Assistant Professor Nagarajan Gnanasekaran gnanasekaran@nitk.edu.in Department of Mechanical Engineering, National Institute of Technology Karnataka, Surathkal, Mangalore 575025, India.

## Nomenclature

| | |
|---|---|
| A | mushy zone constant |
| $a_{sf}$ | interfacial surface area, 1/m |
| $b_f$ | fin thickness, mm |
| $b_s$ | substrate thickness, mm |
| C | inertial resistance, 1/m |
| $c_p$ | specific heat, kJ/(kg·K) |
| $d_f$ | fiber diameter, m |
| $d_{pr}$ | pore diameter, m |
| $\vec{g}$ | acceleration due to gravity, m/s$^2$ |
| H | Enthalpy, J/kg |
| $h_f$ | fin height, mm |
| $h_{fill}$ | foam filling height, mm |
| $h_{ref}$ | reference enthalpy, J/kg |
| $h_s$ | sensible enthalpy, J/kg |
| $h_{sf}$ | interstitial heat transfer coefficient, W/(m$^2$·K) |
| K | Permeability, m$^2$ |
| k | thermal conductivity, W/(m·K) |
| L | latent heat of fusion, kJ/kg |
| LTE | local thermal equilibrium |
| LNTE | local thermal non equilibrium |
| $M_{max}$ | maximization of melting time |
| Mt | melting time, s |
| $P_i$ | performance score |
| P | Pressure, N/m$^2$ |
| $p_f$ | fin positioning |
| PCM | phase change material |
| PV | photovoltaic |
| PPI | pores per inch |
| Pr | Prandtl number |
| Re | Reynolds number |
| $S_{min}$ | minimization of solidification time |
| St | solidification time, s |
| $S^+$ | positive Euclidean distance |
| $S^-$ | negative Euclidean distance |
| T | Temperature, K |
| TOPSIS | technique for order performance by similarity to ideal solution |
| t | Time, s |
| $T_l$ | liquidus temperature, K |
| $T_m$ | melting temperature of PCM |
| $T_r$ | reference temperature, K |
| $T_s$ | solidus temperature, K |
| u,v | velocity in x and y direction, m/s |
| $\vec{v}$ | velocity vector |
| V | weighted normalized values |
| $V^+$ | ideal best value |
| $V^-$ | ideal worst value |
| x,y | spatial coordinates, m |

***Greek symbols***

| | |
|---|---|
| $\varepsilon$ | porosity |
| $\rho$ | Density, kg/m$^3$ |
| $\mu$ | dynamic viscosity, kg/(m·s) |
| $\beta_0$ | coefficient of thermal expansion, 1/K |
| $\Phi$ | liquid fraction |
| $\lambda$ | constant |
| $\varphi$ | porosity of composite |

***Subscripts***

| | |
|---|---|
| eff | effective |
| f | fluid |
| i | rows |
| l | liquid state |
| m | melting |
| mf | metal foam |
| n | total number of values |
| p | PCM |
| s | solidification |

***Superscript***

| | |
|---|---|
| — | normalization |

proposed foam structure can reduce the temperature rise for a prolonged period. Zhao et al. [24] incorporated PCM with partially filled metal foams to minimize the charging and discharging cycle. Four scenarios were investigated in their study such as foams filled separately at the top, bottom, left, and right of the enclosure. An expression for the complete melting time was also proposed for a foam inserted PCM tank.

In order to achieve an enhanced thermal output, several authors have combined two or more enhancers to form a hybrid PCM-based heat sink. The shell and tube heat exchanger was incorporated with nanoparticles, metal foams, and multiple PCMs to recover higher energy from PCM enclosures [25]. The addition of two or more PCM than a single PCM to the heat sink expedites the solidification rate. Further addition of nanoparticles and metal foams accelerates the discharging cycle to a greater extent. Moreover, the metal foam with multiple PCM displays the best thermal performance. Similarly, Xu and Zhao [26] introduced a cascaded thermal energy storage system with multiple PCM. They also derived an analytical solution for temperatures of heat transfer fluid and PCM. Mahdi and Nsofor [27], the authors inserted fins along with foam strips in a PCM-filled shell and tube heat exchanger. Comparatively, the uneven distribution of the fin-foam strip provides adequate performance for both melting and solidification. The heat storage capacity rises depending on the type and the volume fraction of additives added to the system. Refaey et al. [28] developed a storage system for solar photovoltaic (PV) cells combining nanoparticles with PCM and cylindrical fins. Three PCM with different melting temperatures pure and mixed with $Al_2O_3$ are selected and their effects for varying climatic conditions are studied. With the addition of nanoparticles, the life cycle of the solar PV cell improved significantly.

Similarly, a combination of fins and nano-platelets for the extended life of the system was studied [29]. The combined effect of fins and nano additives

strengthen the melting and shrink the resistance offered. Abandani and Ganji [30] studied the performance of a triplex heat exchanger with a combination of metal foams and multiple PCM. The variation of fluid inlet temperature and the porosity range impact the system significantly. Ren et al. [31] developed a heat pipe-assisted PCM-based heat sink and foam-nano particle combination. Immersed boundary-lattice Boltzmann method is used to investigate the PCM melting performance. The results indicate that when there is a rise in radius of the heat pipe, the melting is accelerated until it reaches the critical radius. The nanoparticles effect is diminished when it is incorporated with metal foams. The latter has better enhancement of the melting process.

Nagose et al. [32] used a genetic algorithm approach to find the optimal configuration of PCM-based heat sinks to increase the operating temperature of the sink. Two correlations were proposed, based on the results to relate the parameters considered. For a shell and tube heat exchanger, to accelerate the melting and solidification, Pizzolato et al. [33] presented a topology optimization. The objective is based on the structure of the fins provided in the enclosure. The charging and the discharging cycles can be increased by convective transport with an optimal fin shape. They also found a modified version of the fin structure for easy manufacturing. A straight forward approach to finding a reduced sink height was proposed by Levin et al. [34]. In this study, the number of fins, PCM percentage, and thickness of fins were varied. In their study, the PCM does not melt entirely when the sink reaches critical time due to the wide melting range of PCM used. A tress-shaped fin structure using topology optimization was developed by Xie et al. [35]. The authors investigated the PCM chamber with different orientations and configurations numerically. Augspurger et al. [36] designed an optimal PCM-based system using a dynamic kriging approach. High aspect ratio heat sink provides high velocity within PCM. From their discussions, it is disclosed that the overall configuration of the setup plays a vital role in designing finned heat sinks. Based on the figure of merit approach, Singh et al. [37] designed an optimal composite PCM-based heat sink. The balance between the effective thermal conductivity and the energy storage capacity is considered here. The design points considered are the total volume of composite and interfacial heat transfer area.

This paper combines metal fins with a porous matrix for an efficient thermal outcome of a PCM-based heat sink. The geometry comprehends a PCM-filled chamber with horizontal fins from the sidewalls and a partially filled metal foam to constitute a hybrid enclosure. The main objective of the present study is to provide a multi-objective optimization on a hybrid heat sink filled with PCM. The foam placed contains pores per inch (PPI) ranging from 5-25 with varying porosity 0.8-0.95. Since foams are partially filled, the filling height of foams also varied by 10, 20, and 30 mm. The positioning of the horizontal fin from the top wall and fin height is also estimated initially and fixed later for the variation of foam analysis. A total of 60 cases was developed and analyzed for the charging and discharging cycle using Ansys Fluent. A constant hot wall temperature of 50 °C is applied at the bottom of a heat sink with the rest of the walls insulated. From the studies, it is seen that the technique for order performance by similarity to ideal solution (TOPSIS) algorithm for a PCM-based heat sink is scarce. Maximizing melting time ($M_{max}$) and minimizing solidification time ($S_{min}$) are the objective functions considered during optimization. The outcome from the descriptions can provide a broad knowledge of picking the right porous structure when inputting partial filling.

## Numerical description

A rectangular enclosure of $104 \times 52$ mm with 2 mm substrate thickness ($b_s$) is numerically developed from the past study [38]. For effective cooling performance, both the fin and foams are employed as thermal enhancers in the heat sink. As shown in Figure 1, fins are placed horizontally at the sidewall of the enclosure, and the metal foam is placed at the bottom. The solid material chosen is aluminum for fins, foams, and substrate. A heat spreader is imparted to the PCM cavity as a substrate for uniform heat dissipation. PCM used in the current study is n-eicosane, and the PCM cavity dimensions are $50 \times 100$ mm. The properties of PCM used are listed in Table 1 [38]. Due to its symmetrical nature, only half of the enclosure is considered to reduce the computational time.

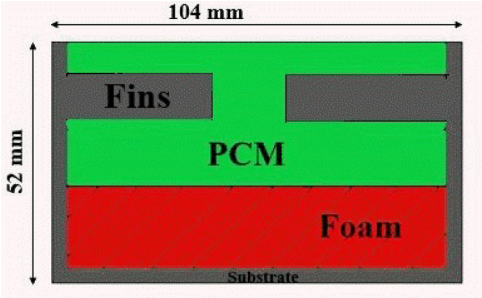


Figure 1. Two-dimensional enclosure.

A computational domain for numerical study is provided in Figure 2.

Overall, 60 cases are considered in this study to select an optimum design by varying the parameters. The parameters accounted for are filling height ($h_{fill}$), foam porosity ($\varepsilon$), and foam density. The heights of the foam-filled in the heat sink are 10, 20, and 30 mm. The range of the porosity of foam is 0.8-0.95 with increasing order of pore density from 5 PPI to 25 PPI. Based on the completion of the charging and discharging cycles, the study is undertaken from these parameters. Two models are involved when the investigation is done on a porous matrix-based heat sink. One is the local thermal equilibrium model (LTE), and the other is the local non-thermal equilibrium model (LNTE). In the LTE model, an identical temperature between the foams and fluids is noticed. It explains that a single set of energy transport equations is employed for this model. Whereas for the LNTE model, two different unique energy transport equation is applied. Accordingly, a dissimilar temperature is found between the foams and fluids within the enclosure. Here, LNTE is preferred with enthalpy porosity formulation for a porous filled PCM-based heat sink. Boussinesq approximation in the liquid state of PCM with density variation to account for natural convection is employed. The fluid is considered Newtonian and incompressible. A laminar and unsteady state for the fluid flow with homogenous and isotropic properties for PCM and foam are considered. During the phase change, the properties such as thermal conductivity, specific heat, and viscosity are kept constant. The shrinkage of PCM volume during solidification and expansion of PCM volume during melting are neglected.

**Table 1.** Properties of materials [38].

| Properties | Units | n-eicosane | Aluminum |
|---|---|---|---|
| Density, $\rho$ | kg/m$^3$ | 780 | 2719 |
| Thermal conductivity, k | W/m·K | 0.16 | 202.4 |
| Specific heat, $c_p$ | kJ/(kg·K) | 2200 | 871 |
| Dynamic viscosity, $\mu$ | kg/(m·s) | 0.00355 | – |
| Melting temperature, $T_m$ | °C | 36.5 | – |
| Latent heat of fusion, L | J/kg | 237,000 | – |
| Coefficient of thermal expansion, $\beta_0$ | 1/K | 0.001 | – |

## Governing equations

The governing equations about the analysis consist of continuity, momentum, and energy equations given in Eqs. (1)–(4). "A" in the momentum equation is the mushy zone parameter that controls the damping of velocity conversion during solidification. It usually ranges from $10^4$ to $10^7$, and from the studies, the preferable value is $10^5$ [39, 40]. $\lambda$ is a constant value of 0.001, and its purpose is to elude zero in the denominator.

The governing equations are considered from [41] when only fins are considered with PCM at first, and the subscript p denotes PCM.

Continuity and momentum equations:

$$\frac{\partial \rho_p}{\partial t} + \frac{\partial (\rho_p u)}{\partial x} + \frac{\partial (\rho_p v)}{\partial y} = 0 \tag{1}$$

$$\rho_p \frac{D\vec{v}}{Dt} = \mu \nabla^2 \vec{v} - \nabla P + \rho_p \beta_0 (T_m - T) \vec{g} + A \frac{(1-\Phi)^2}{(\Phi^3 + \lambda)} \vec{v} \tag{2}$$

Energy equation:

$$\Phi = 0, \ if \ T < T_s \tag{3.a}$$

$$\Phi = 1, \ if \ T > T_l \tag{3.b}$$

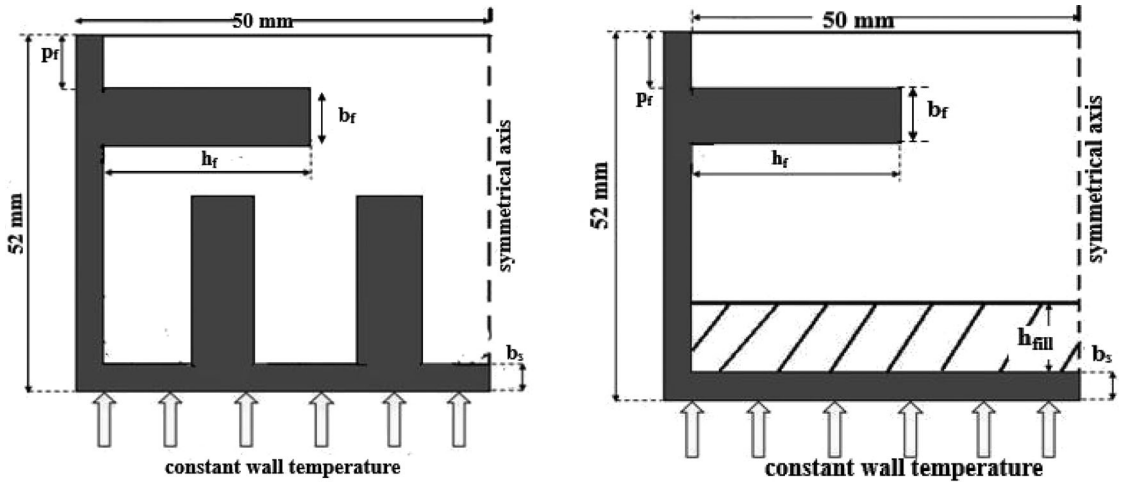


**Figure 2.** Computational domain of hybrid heat sink (a) with only fins and (b) with fins and foams.

$$\Phi = \frac{T - T_s}{T_l - T_s} \quad if \quad T_s < T < T_l \tag{3.c}$$

$$\frac{\partial}{\partial t}(\rho H) + \nabla \cdot \left(\rho \vec{v} H\right) = \nabla \cdot (k \nabla T) \tag{4}$$

The liquid fraction of PCM is given by Φ; this gives how much the amount of PCM melts in a unit cell. Where 0 determines PCM still in the solid phase, and one shows the PCM melted completely. The value between regions 0 and 1 leads to a mushy zone, where the PCM is semi-solid. The liquid fraction for varying temperature is given in Eq. (3 a-c). In Eq. (4), H denotes enthalpy, and it accounts for both sensible and latent enthalpy. $T_r$ is the reference temperature in Eq. (6), with this reference temperature reference enthalpy is derived ($h_{ref}$).

$$H = h_s + \Phi L_l \tag{5}$$

$$h_s = h_{ref} + \int_{T_r}^{T} c_p \mathrm{dT} \tag{6}$$

When the cases with foams are introduced with the PCM, the governing equations are modified. In combination of both PCM and metal foams (mf) are derived below [41],

Continuity equation:

$$\frac{\partial \rho_p}{\partial t} + \frac{\partial(\rho_p u)}{\partial x} + \frac{\partial(\rho_p v)}{\partial y} = 0 \tag{7}$$

x-Momentum equation

$$\frac{\rho_p}{\varphi}\left\{\frac{\partial u}{\partial t} + \frac{1}{\varphi}\left(u\frac{\partial u}{\partial x} + v\frac{\partial u}{\partial y}\right)\right\} = -\frac{\partial P}{\partial x} + \frac{\mu}{\varphi}\left(\frac{\partial^2 u}{\partial x^2} + \frac{\partial^2 v}{\partial y^2}\right) + \frac{(1-\Phi)^2}{\Phi^3 + \lambda}\ \mathrm{A}u - \frac{\mu}{K}u - \frac{1}{2}C\rho_p u|u| \tag{8}$$

y-Momentum equation:

$$\frac{\rho_p}{\varphi}\left\{\frac{\partial v}{\partial t} + \frac{1}{\varphi}\left(u\frac{\partial v}{\partial x} + v\frac{\partial v}{\partial y}\right)\right\} = -\frac{\partial P}{\partial y} + \frac{\mu}{\varphi}\left(\frac{\partial^2 u}{\partial x^2} + \frac{\partial^2 v}{\partial y^2}\right) + \frac{(1-\Phi)^2}{\Phi^3 + \lambda}\ \mathrm{A}v - \frac{\mu}{K}v - \frac{1}{2}C\rho_p v|v| + \rho_p \beta_0\ (T_m - T)\ \vec{g} \tag{9}$$

Energy equation:

$$(1-\varepsilon)(\rho c_p)_{mf}\frac{\partial T_{mf}}{\partial t} = k_{eff_{mf}}\left(\frac{\partial^2 T_{mf}}{\partial x^2} + \frac{\partial^2 T_{mf}}{\partial y^2}\right) + h_{sf}a_{sf}\left(T_P - T_{mf}\right) \tag{10}$$

$$\varepsilon(\rho c_p)_P\frac{\partial T_P}{\partial t} + \varepsilon(\rho c_p)_P\left(u\frac{\partial T_P}{\partial x} + v\frac{\partial T_P}{\partial x}\right) = k_{eff_p}\left(\frac{\partial^2 T_P}{\partial x^2} + \frac{\partial^2 T_P}{\partial y^2}\right) + \varepsilon\rho_p L_p\frac{\partial \Phi}{\partial t} + h_{sf}a_{sf}\left(T_{mf} - T_P\right) \tag{11}$$

The composite porosity is indicated by $\varphi$. The terms 4 and 5 on the right side of the momentum equation determine the flow within the open porous medium. The Darcy, non-Darcy, and inertial effects of metal foam are provided by Darcy-Forchheimer law. The main parameters in the metal foam structure investigations are interfacial surface area ($a_{sf}$), permeability (K), and inertia coefficient (C). Equation (12), the interfacial surface area is derived from Calmidi and Mahajan [42]. It is defined as the surface area ratio between the void and ligaments to the total unit cell volume. The pressure gradient developed when the fluid flows through the porous medium is permeability. The term inertia coefficient explains the resistance offered by the metal foam due to its complex structure. The widely used correlations for permeability and inertia coefficient [43] are reported in Eqs. (16) and (17). Since PCM and solid foams are employed, there is a need to find an effective thermal conductivity. Though there are numerous empirical and analytical correlations proposed by the authors, in this study $K_{eff}$ is evaluated from the correlations proposed by Boomsma and Poulikakos [44]. The last key parameter is the interstitial heat transfer coefficient ($h_{sf}$), which assesses the energy interaction between metal structures and PCM; fiber diameter ($d_f$), and pore diameter ($d_{pr}$) in Eqs. (13–15) also derived from correlations of [45].

$$a_{sf} = \frac{3\pi d_f(1 - \exp - ((1-\varepsilon)/0.04))}{(0.59 d_{pr})^2} \tag{12}$$

$$\frac{h_{sf}d_f(1 - \exp - ((1-\varepsilon)/0.04))}{k_f} = \begin{cases} 0.76 Re_{df}^{0.4} Pr^{0.37}, & (1 \le Re_{df} \le 40), \\ 0.52 Re_{df}^{0.5} Pr^{0.37}, & (40 \le Re_{df} \le 10^3), \\ 0.26 Re_{df}^{0.6} Pr^{0.37}, & (10^3 \le Re_{df} \le 2 \times 10^5). \end{cases} \tag{13}$$

$$d_{pr} = \frac{0.0254}{PPI} \tag{14}$$

$$\frac{d_f}{d_{pr}} = 1.18\sqrt{\frac{1-\varepsilon}{3\pi}} \times \frac{1}{1 - \exp - ((1-\varepsilon)/0.04)} \tag{15}$$

$$K = 0.00073(1-\varepsilon)^{-0.224}(d_f/d_{pr})^{-1.11} {d_{pr}}^2 \tag{16}$$

$$C = 0.00212(1-\varepsilon)^{-0.132}(d_f/d_{pr})^{-1.63} \quad (17)$$

## Grid independence study and validation

The numerical simulations are carried out in ANSYS Fluent 19, which is based on the finite volume method. A grid size study and a time step size study are performed to obtain numerical accuracy. The liquid fraction is plotted in Figure 3, for the hybrid heat sink with varying time periods by fixing filling height 30, porosity 0.8, and 5 PPI. For the grid size study, the time step size is fixed at 0.5 s and the element size considered are 15000, 20000, and 25000.

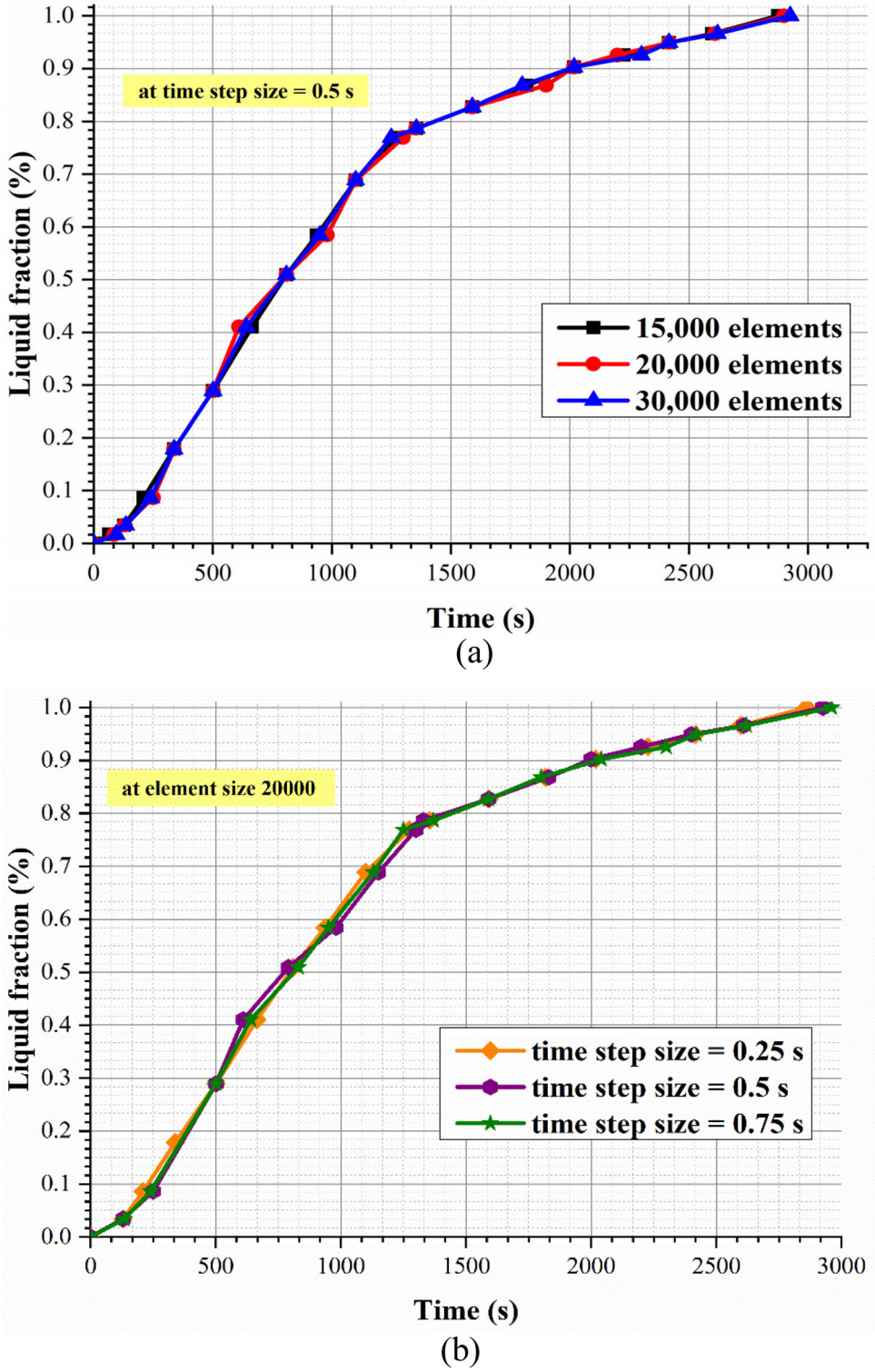


Figure 3. Grid independence study (a) Element size study and (b) Time step size study.

Element size is set at 20000 by varying time step size from 0.25 s, 0.5 s, and 0.75 s. The time step size and number of elements selected for the forthcoming simulations are 0.5 s and 20000.

The validation of this numerical methodology is done by comparing the work carried out by Zheng et al. [46]. Paraffin wax is filled in an enclosure with copper metal foams. The porosity 0.95 and pore density of 5 PPI of copper foam are kept constant, and studies are done. The temperature variation within the PCM in the enclosure results is compared in Figure 4. The left side of the enclosure is heated at a constant heat flux of 1150 W/m$^2$. The remaining walls are kept in adiabatic conditions, apart from the heating side.

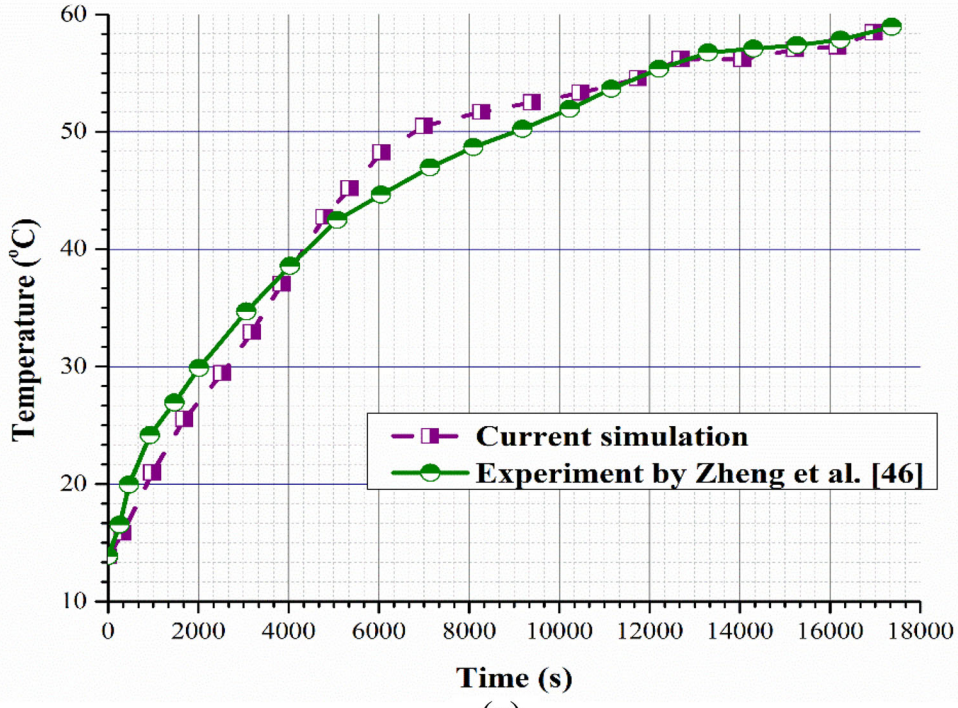


**Figure 4.** Numerical validation (a) melting process [46] and (b) solidification process [25].

Initially, the paraffin PCM is at the temperature of 15°C under no-slip conditions. The experiment was repeated twice under the same conditions to ensure accuracy. The total uncertainty of the experiment was around 7.04%, including power inputs (2%), thermocouples (0.4%) and heat loss (4.6%). A maximum deviation of 8% around 6000s is found when simulation results are compared with the experimental study. This deviation is due to the thermal properties of the materials used. In experiments, the thermal properties vary with time, but these properties are kept constant in numerical studies.

Next, for the validation of solidification process, a multiple PCM case is considered. The results of freezing process from numerical studies by Mahdi et al. [25] are compared with the present numerical work. The heat sink is filled with three different PCM of RT-55, RT-60, and RT-65. In shell and tube heat exchanger, with initial temperature of 353 K, and leaving the surface temperature to ambient, the simulations are carried out. The remaining walls are kept at adiabatic conditions. From the results, the liquid fraction is plotted for various time interval and an average deviation of 3.2% is observed.

## TOPSIS

Technique for order performance by similarity to ideal solution (TOPSIS) is a versatile multi-objective tool that eases the analysis under circumstances where both desired and undesired outcomes are accompanied. Previous studies have successfully applied it to comprehensively analyze various tradeoffs between heat transfer maximization and flow resistance minimization in metal foams [47, 48]. This method permits various weightages on the ability to maximize the desired outcome and on the ability to minimize the undesired outcome, thereby allowing comprehending the effect of introduced variable conditions.

The present study shows that the advantage of a decrease in solidification time with the use of metal foams with PCM as a result of enhanced heat transfer comes with the disadvantage of decreased melting time. However, the key point is the optimal solidification and melting time. In the present study, various parameters such as fin height, positioning of fins, and metal foams of altered structural combinations (porosity and pore density) are considered, and variations in melting and solidification time are witnessed. However, the tradeoff between melting and solidification time must be well understood to comprehensively analyze the outcomes. Techniques like TOSPIS enable one to analyze such conditions where introducing/variation in individual parameters results in both desired (reduction in solidification time) and undesired (reduction in melting time) phenomena mainly due to enhanced heat transfer. Through the TOPSIS method, the outcomes of the present work, i.e., melting time and solidification time with variation in considered parameters such as varying porosity and pore density combinations of metal foams and fin height, are analyzed subjected to various criteria. Each criterion is adopted based on different weightages placed on maximizing the desired outcome, which is enhancing melting time and minimizing undesired effect, which is reducing solidification time. In the present work, varied parameters such as metal foam properties, fin height, and positioning of the fin are analyzed in combination with PCM, and the TOPSIS method is implemented to comprehend the tradeoff between melting time and solidification time

Various steps involved in implementing the TOPSIS method are as follows [48]:

- Step 1:
  Compute columns comprising values of melting time ($Mt_{i1}$) and solidification time ($St_{i2}$). Then extend it to two more columns, each comprising normalized magnitudes of values in the first two columns ($\overline{Mt_{i3}}$) and ($\overline{St_{i4}}$) respectively using Eqs. (18) and (19).

$$\overline{Mt_{i3}} = \frac{Mt_{i1}}{\sqrt{\sum_{i=1}^{n} {Mt_{i1}}^2}} \tag{18}$$

$$\overline{St_{i4}} = \frac{St_{i2}}{\sqrt{\sum_{i=1}^{n} {St_{i2}}^2}} \tag{19}$$

  where, $i = 1, 2, \ldots \ldots, n$, implying the rows and 'n' referring to a total number of values (corresponding to all variable conditions).

- Step 2:
  Various weights are added to the weighted normalized values, using Eqs. (20) and (21). The distributed weight varying from 0 to 1 is assigned to the previously computed normalized values of melting and solidification based on desired tradeoff scenario.

$$V_{i5} = \overline{Mt_{i3}}.W_m \tag{20}$$

$$V_{i6} = \overline{St_{i4}}.W_s \tag{21}$$

  $W_m$ and $W_s$ are 0 and 1 for criteria I, 0.25 and 0.75, 0.5 and 0.5, 0.75 and 0.25 and 1 and 0 for criteria II, III, IV, and V, respectively.

- Step 3:
  Compute ideal worst and ideal best values. Since solidification time is considered as a non-beneficial parameter as it is expected to be minimized while melting time is considered as the beneficial parameter as it is expected to be maximized, the highest value from the weighted normalized values of solidification time is treated as the ideal worst, while the lowest value from the weighted normalized values of solidification time is treated as ideal best. On the other hand, the highest value from the weighted normalized values of melting time is considered as ideal best, while the least value from the weighted normalized values of melting time is considered as ideal worst as expressed in Eqs. (22)–(25).

$$V_m{}^{+} = \max(V_{i5}) \tag{22}$$

$$V_s{}^{+} = \min(V_{i6}) \tag{23}$$

$$V_m{}^{-} = \min(V_{i5}) \tag{24}$$

$$V_s{}^{-} = \max(V_{i6}) \tag{25}$$

- Step 4:
  Compute Euclidean distance, which refers to the relative distance of individual values in a weighted normalized column from the ideal values identified (best or worst). Positive Euclidean distance corresponds to the distance of each value in the weighted normalized column from the ideal best value and is calculated as given in Eq. (26). Similarly, negative Euclidean distance is the distance of each value in the weighted normalized column from the ideal worst value and is calculated as given in Eq. (27).

$$S_i{}^{+} = \left[(V_{i5} - V_m{}^{+})^2 + (V_{i6} - V_s{}^{+})^2\right]^{0.5} \tag{26}$$

$$S_i{}^{-} = \left[(V_{i5} - V_m{}^{-})^2 + (V_{i6} - V_s{}^{-})^2\right]^{0.5} \tag{27}$$

- Step 5:
  Performance scores of each variable condition are evaluated using Eq. (28). It ranks the considered varying states based on their closeness in meeting the fixed weighted criteria.

$$P_i = \frac{S_i{}^{-}}{S_i{}^{+} + S_i{}^{-}} \tag{28}$$

## Evaluation of fin placement and height

The steps involved in the numerical procedures are represented as flow chart in Figure 5. The governing equations comprising PCM are solved using finite volume method based ANSYS Fluent software. In this simulation, the methods applied for pressure-velocity coupling are SIMPLE algorithm and PRESTO! Scheme for pressure correction equation. A second-order upwind scheme is specified in consideration of the discretization of momentum and energy equations. The relaxation factors default values are set for the pressure, momentum, liquid fraction, and energy. A constant value of $10^{-6}$ is assorted for both continuity and momentum equations. Whereas for the energy equation, a value of $10^{-8}$ is specified.

Initially, to determine the height of the fin and positioning of the horizontal fin, few cases were selected and given in Table 2. In these cases, only fins were selected to acquire the behavior of PCM, and foams were neglected. Since the fin height varies, the thickness of the fin also varies accordingly, but the area of the fin remains constant. The selected geometry is given in Figure 1. Three conditions are selected; first, the importance is given to minimization of solidification time completely. In the second condition B, the importance is shared equally between both the objective function of maximizing melting time and minimizing solidification time. And finally in the condition C, the importance is set entirely for the maximization of melting. TOPSIS algorithm is applied to find the best fit among the different cases. The fin positioning and fin height are varied for rectangular shapes, and results are obtained.

From the results for all weightages in Table 3, it is clear that the rectangular fin shape impacts the system significantly. This is because rectangular fin shapes have a uniform thickness throughout the enclosure, which dissipates uniform heat flow. Hence, heat flow is enlarged for rectangular fins within the PCM and accelerates the process. Similarly, considering fin height 25 mm for the first two conditions yield better results. This is due to the increased fin height; the amount of heat conducted within PCM also increases, thus accelerating the process. But for condition C, when the importance is solely set to maximization of melting, lesser fin height delivers a greater outcome because its lesser amount exists within the PCM cavity. Subsequently, setting the horizontal fins from the top wall, for the first two conditions 11 mm, significantly influences the process. When the fin is near the top wall, it affects the natural convection remarkably; as a result, the process is expedited. Inversely, when the fins are placed away from the top wall, it decelerates the melting. Therefore, when the weightage is prolonged melting, 13 mm delivers an extended melting time.

The statement above conveys a clear idea of the placement of horizontal fins at 11 mm from the top wall and the height of fins to be 25 mm. With the

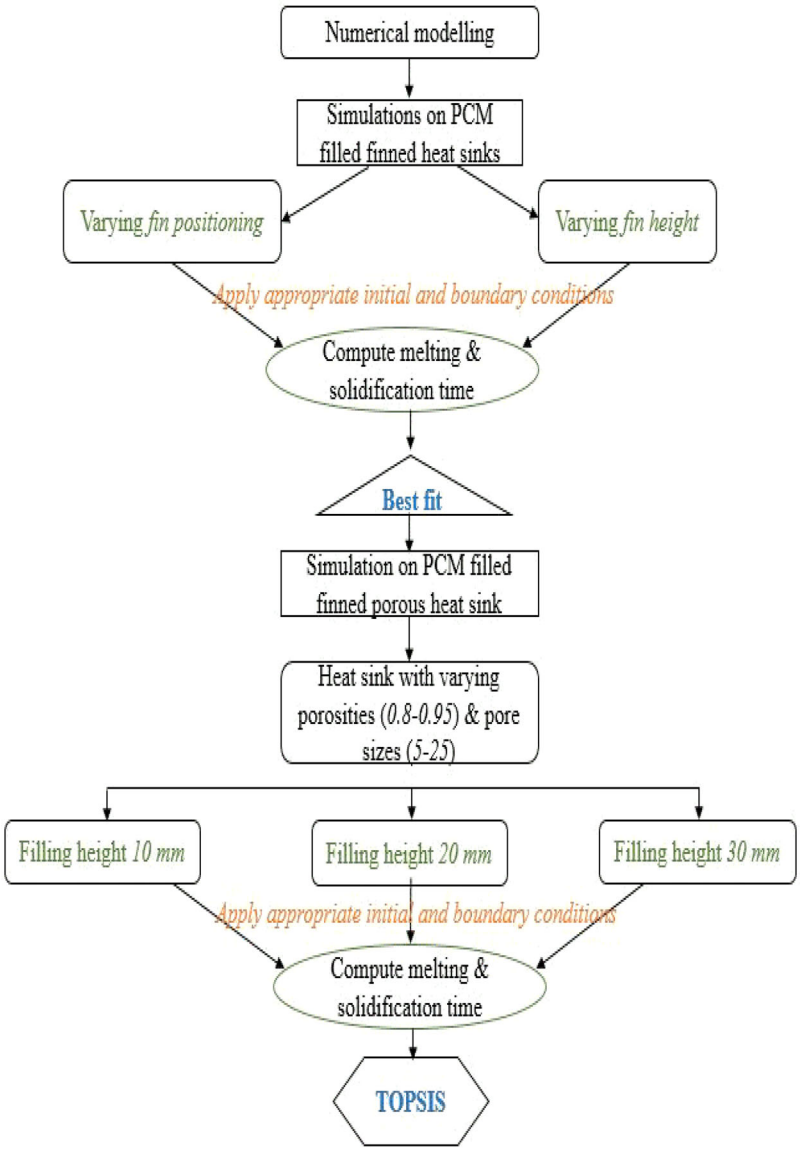


**Figure 5.** Flowchart with numerical procedure.

**Table. 2** Case study with only finned PCM heat sink.

| Cases | | Rectangular fins | |
|---|---|---|---|
| A ($p_f = 13$ mm) | 1 | 2 | 3 |
| | $h_f = 16$ mm | $h_f = 20$ mm | $h_f = 25$ mm |
| B ($h_f = 20$ mm) | 1′ | 2′ | 3′ |
| | $p_f = 11$ mm | $p_f = 13$ mm | $p_f = 15$ mm |

**Table 3.** Responses for fin positioning and fin height.

| Weightage | Parameters | Best fit | Worst fit |
|---|---|---|---|
| Condition A | $p_f$ | 11 mm | 13 mm |
| $M_{max} : S_{min} = 0{:}1$ | $h_f$ | 25 mm | 16 mm |
| Condition B | $p_f$ | 11 mm | 13 mm |
| $M_{max} : S_{min} = 0.5{:}0.5$ | $h_f$ | 25 mm | 16 mm |
| Condition C | $p_f$ | 13 mm | 15 mm |
| $M_{max} : S_{min} = 1{:}0$ | $h_f$ | 16 mm | 25 mm |

variation of fin height, fin thickness also varies, and at 25 mm height, the thickness is 5.6 mm. Following this, our main goal to obtain optimized partially filled metal foam with a finned heat sink is assessed. Zhu et al. [49] studied the effect of partial filling of foams in a PCM-based heat sink. Their communications stated that fully filling of foams can be uneconomical and the weightage of the heat sink also became critical. Hence in this work, a feasible strategy of encompassing the partial filling of foams with fins on a PCM-based enclosure is examined.

## Results and discussion

### *Initial and boundary conditions*

The heat is dissipated from the bottom side, and the rest of the side walls are insulated. During the

charging cycle, the PCM is initially at the solid phase, and the temperature of foam ($T_{mf}$) and the temperature of PCM ($T_p$) are at 27°C. The hot wall side is at a constant wall temperature condition of 50°C. Similarly, during discharging cycle, the bottom wall is kept at 27°C. The PCM is at the liquid state, and the $T_{mf}$ and $T_p$ are at 50°C.

Performance scores define the score based on their results from TOPSIS. These scores give the importance of each parameter and how it contributes to the objective function. The performance scores range from 0 to 1 for different weightage inputs. For any condition, the parameter closer to value 1 has the best fit for a function, and the parameter closer to value 0 has the worst fit. From Table 4, in the first two criteria, the weightages are toward minimizing solidification time. This table is based on the geometry with only fins which is represented in Figure 2(a). Likewise, for the last two criteria, the importance is set to maximize melting time. Especially on criteria-1 and criteria-2, the weightage is solely specified to minimize discharging time and maximization of charging time. Finally, the weightage is distributed only for a prolonged charging cycle at criteria-5.

**Table 4.** Weightage ratio for each criteria.

| Weightage ratio | Criteria-1 | Criteria-2 | Criteria-3 | Criteria-4 | Criteria-5 |
|---|---|---|---|---|---|
| $M_{max}$ | 0 | 0.25 | 0.5 | 0.75 | 1 |
| $S_{min}$ | 1 | 0.75 | 0.5 | 0.25 | 0 |

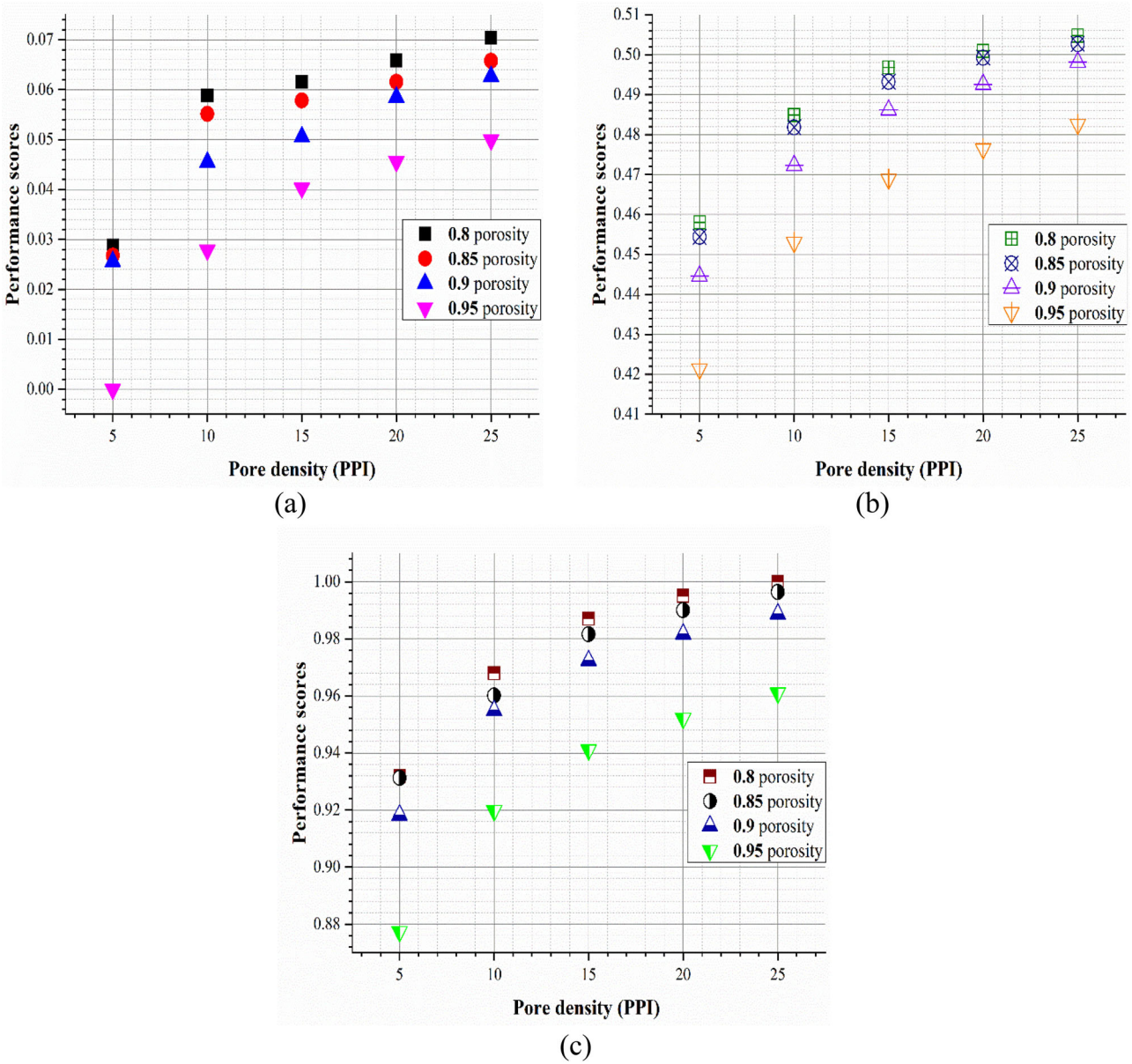


**Figure 6.** Performance scores of Criteria-1 for filling heights (a) 10 mm, (b) 20 mm, and (c) 30 mm.

The aim of the present paper is to obtain better thermal enhancement for melting and solidification. In order to compare the variations in parameters during both cycles, it is required to consider this as a separate process. Only if this is treated as a separate process, one can come to know which is the beneficial and non-beneficial parameters from the results obtained.

### *Criteria-1*

All the criteria (1-5) and its corresponding Figures 6–10 are derived from the geometry of Figure 2(b), where both fin and foams are placed. In criteria-1, the weightage is mainly set to minimize solidification time and no weightage for melting. The filling height is varied as 10, 20, and 30 mm for different porosity and pore densities, and the results are plotted in Figure 6. It is clearly visible from the plots that increment in filling height leads to the desired effect of solidification, and the performance score is also above 0.88 according to Figure 6(c). This is because the amount of foam volume within the heat sink is higher, accelerating solidification. Whereas filling height with 10 mm has more PCM volume and a lesser volume of foams than other filling heights. So, there is a longer solidification period and hence least performance score below 0.07 is observed for 10 mm filling height.

When considering porosity and pore density, 0.8 porosity with 25 PPI provides a better outcome. This is the same for all filling height cases. The reason is compared to 0.95 porosity, 0.8 porosity has a lesser amount of PCM. An increase in void space can fill a larger

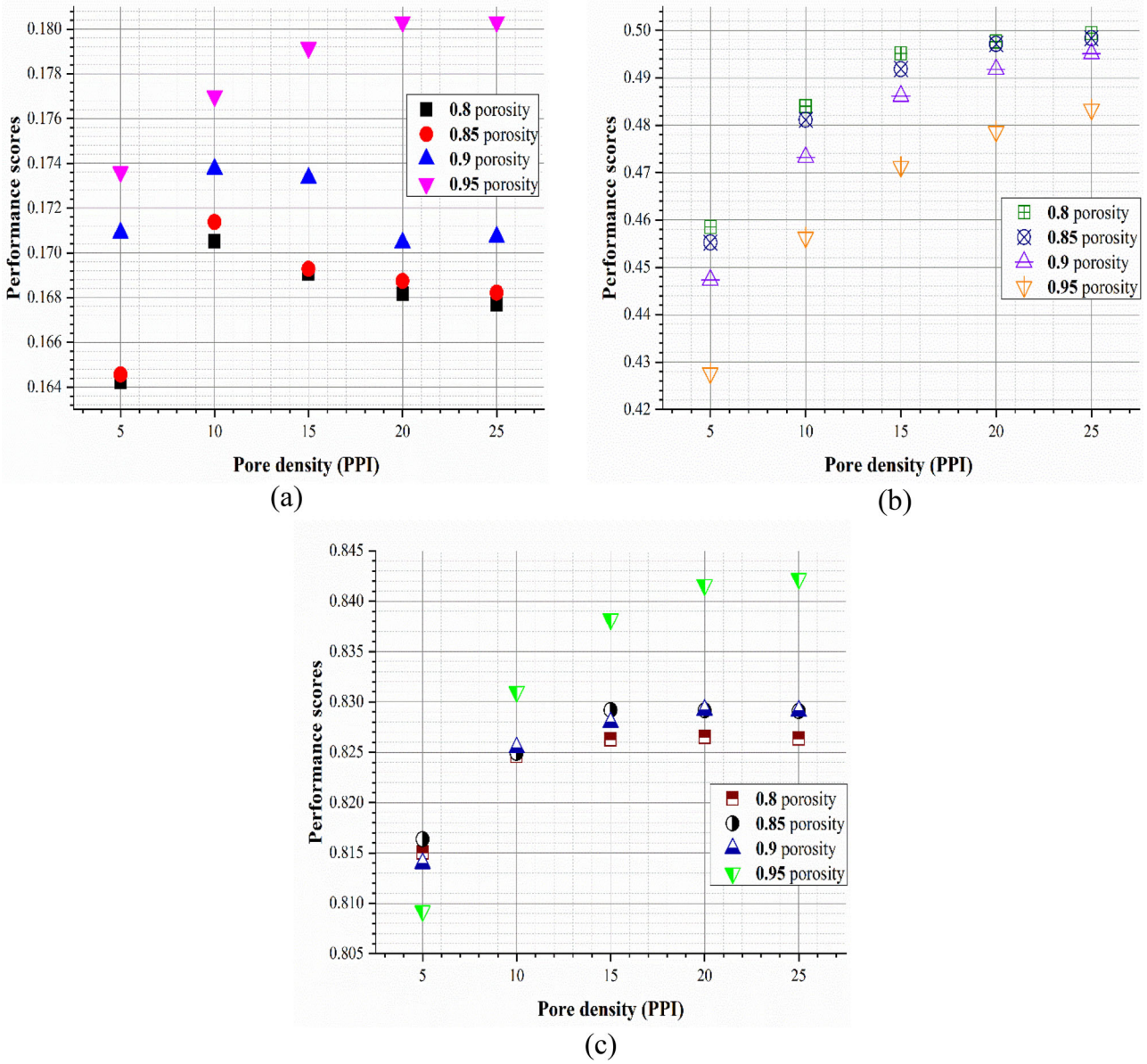


**Figure 7.** Performance scores of Criteria-2 for filling heights (a) 10 mm, (b) 20 mm, and (c) 30 mm.

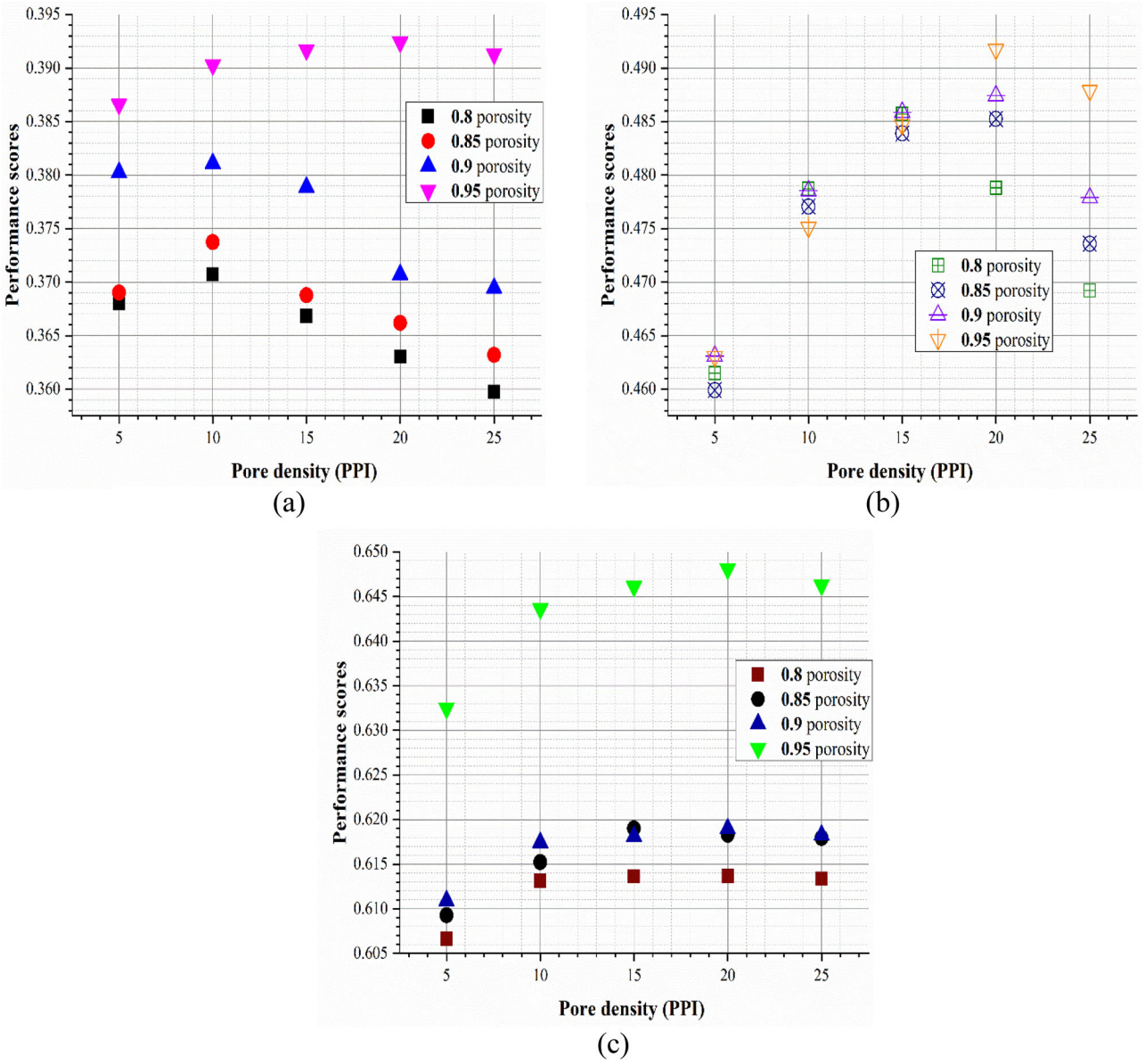


**Figure 8.** Performance scores of Criteria-3 for filling heights (a) 10 mm, (b) 20 mm, and (c) 30 mm.

amount of PCM. Though the difference between scores for 0.8, 0.85, and 0.9 is less, the difference of 0.95 porosity compared with other porosity is large. Similarly, for pore density considering a single unit, the solid structure is higher for higher density. Therefore, 25 PPI yields better results than the other PPI. The trend for all PPI is almost similar at any height.

### *Criteria-2*

In criteria-2, the weightage is mostly inclined toward minimizing solidification time and less toward maximizing melting. Similar to criteria-1 in Figure7, with increment in filling height the solidification time is less. But here quarter amount of weightage is toward the melting time; hence there is a rise in the score for 10 mm filling height and a fall in scores for 30 mm filling height. This explains that when importance is given for both, the objective function filling height considerably impacts the heat sink at these heights. Despite a change in scores for filling heights 10 mm and 20 mm, the performance scores for 20 mm height for both criteria-1 and criteria-2 remain the same.

Correspondingly for varying porosity at 10 mm filling height, except for 0.95 porosity, the trend for remaining porosity increases first and then decreases with an increase in PPI. Besides porosity, the change in PPI does not alter the trend. In parallel to the 10 mm case with varying PPI, for 30 mm filling height apart from 0.95 porosity, remaining all have an increasing trend at the beginning, and then there is a slight decrement toward the end. 0.95 porosity at 25

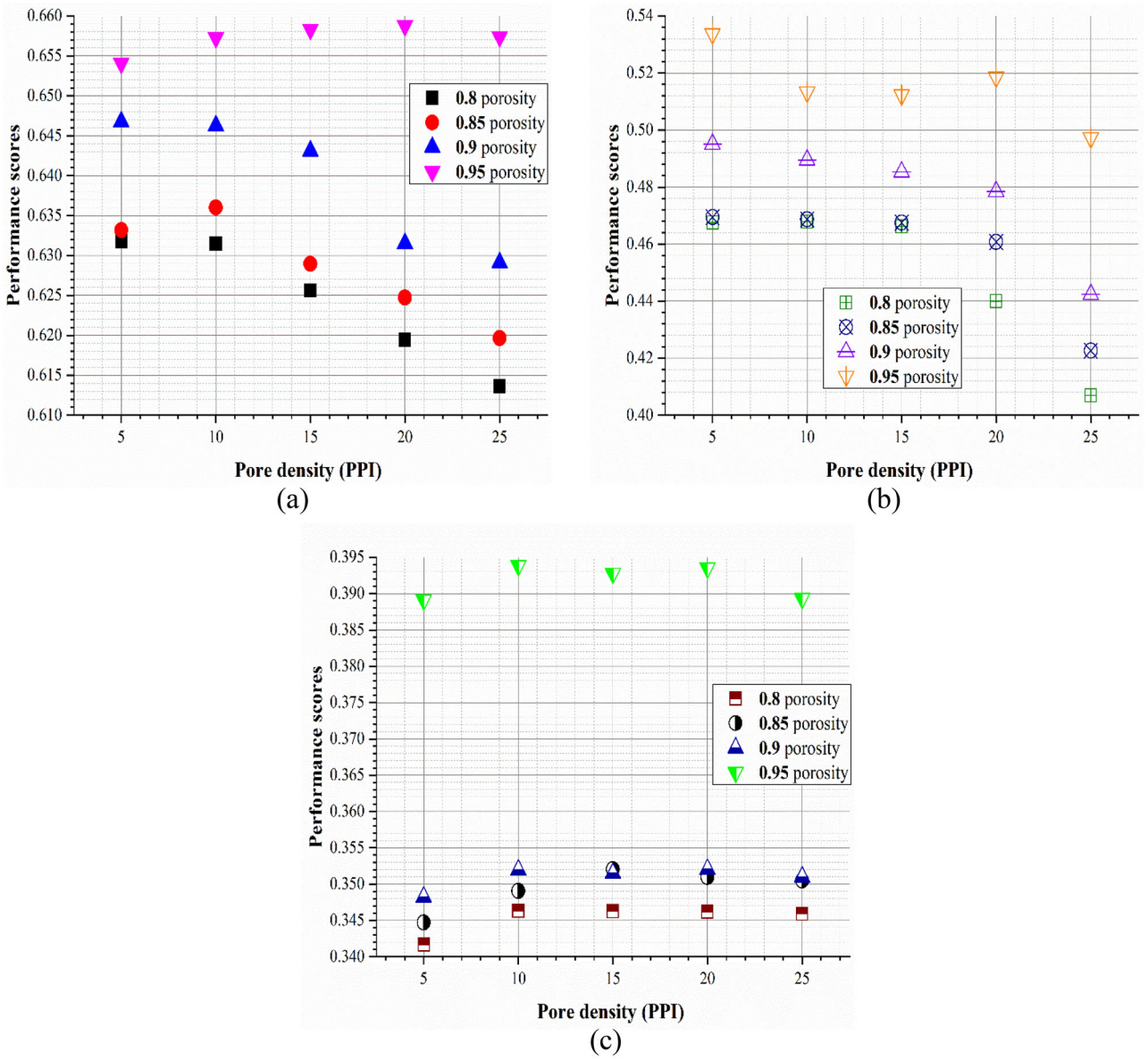


**Figure 9.** Performance scores of Criteria-4 for filling heights (a) 10 mm, (b) 20 mm, and (c) 30 mm.

PPI yields a higher performance score for both cases. But with PPI cases, 0.95 has the least score at 5 PPI, and after that, there is a sudden rise in score. When the weightage of prolonged melting is considered, 0.95 plays a major role. Irrespective of changes found in the 10 mm and 30 mm filling trends, the trend remains the same for all porosity and PPI for 20 mm filling height. Unlike the other two cases, in this 20 mm filling height, 0.8 porosity with 25 PPI has better performance scores.

### *Criteria-3*

Equal importance is given to both objective functions in criteria-3. Here, an aforementioned discussion is applied, i.e., the higher filling foams affect the solidification significantly. But the performance scores observed from the first three criteria show that the outcome score is influenced by different weightage applied. The least performance score has been increased from 0 to 0.6 for the filling height of 10 mm in Figure 8. Inversely for 20 mm filling height, the maximum performance scores decreased from 1 to 0.606. This shows that as the weightage for the given objective function varies the performance outcome also gets affected. Despite this occurrence, the performance scores of filling height with 20 mm remain almost the same for the first three criteria.

A porous structure with 0.95 porosity at 20 PPI has higher performance scores for all three cases. In addition to it, the graph shows a rise initially and then falls for all porosity at 10 mm when there is a change

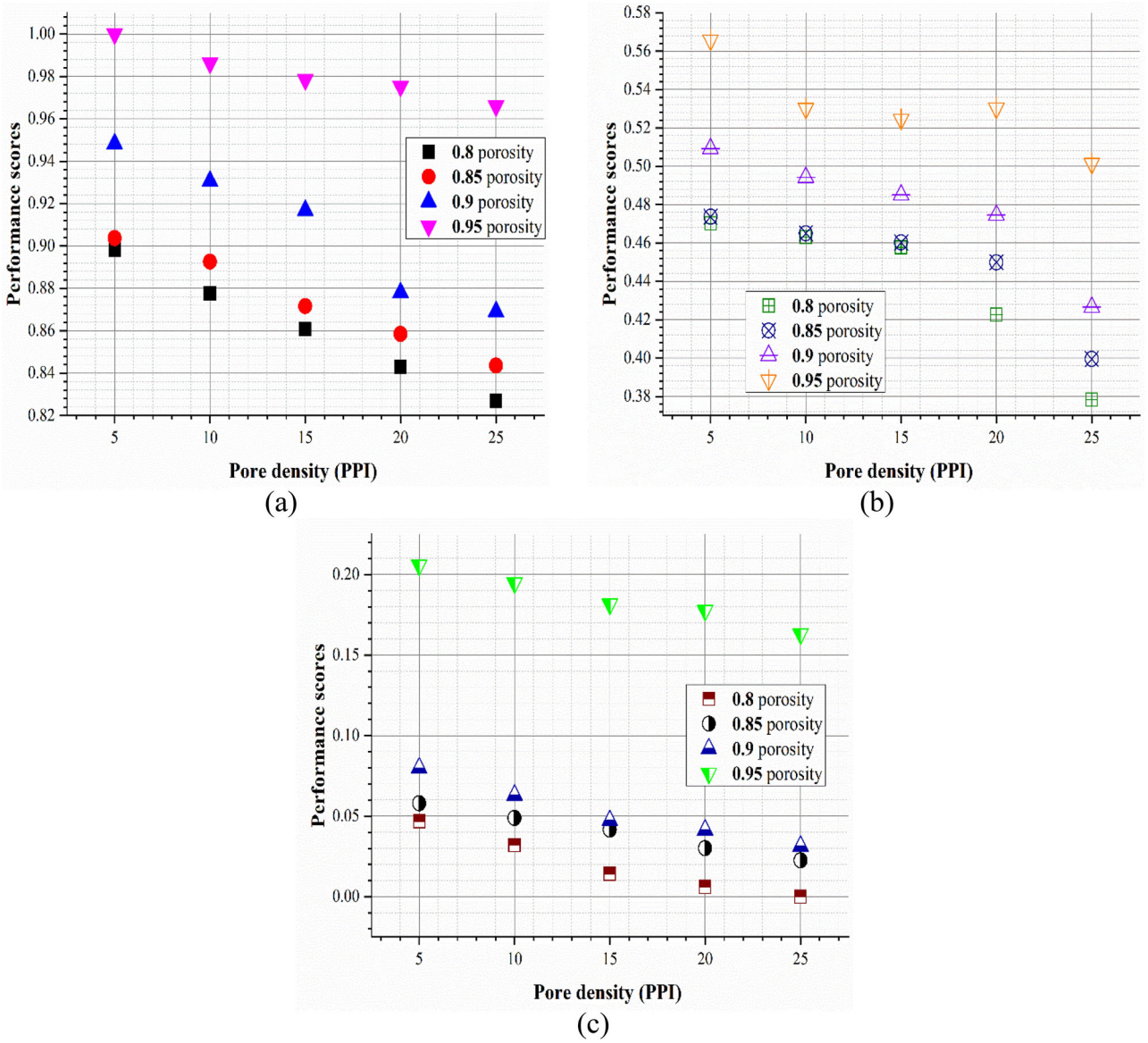


**Figure 10.** Performance scores of Criteria-5 for filling heights (a) 10 mm, (b) 20 mm, and (c) 30 mm.

in PPI. There is a slight decline at 30 mm filling height at the later end of the plots. A non-identical plot is observed for filling height 20 mm; the score is increasing up to 5 PPI, and it drops down at 25 PPI. The cause of this drop is due to the increase of pore density after 20 PPI becomes significant for 20 mm porous height.

### *Criteria-4*

When the weightage is shifted slightly toward the maximization of melting time, low filling foams try to dominate. The performance scores are higher for 10 mm than the other two cases. The explanation for this change is when the filling height decreases, the volume of PCM increases. So, the heat transfer within PCM decreases. Therefore, higher amount of PCM leads to a longer melting period. The maximum performance score is observed in Figure 9 at 10 mm, and the least performance scores are noted at 30 mm. Whereas, for the case of 20 mm the performance scores do not alter highly. But a slight improvement in maximum performance score is spotted at 0.54.

A better response is observed on accounting for the porous structure in criteria-4. For all 3 cases, 0.95 porosity has a desirable outcome with varying porosity. However, when there is a change in PPI, distinct results are observed for each filling height case. When the foams are filled till 10, 20, and 30 mm, 20 PPI, 5 PPI, and 10 PPI induce higher scores, respectively.

### *Criteria-5*

The sole weightage is specified for the melting period elongation at criteria-5. Contrarily to criteria-1, here, null weightage is defined for shortening of solidification time. Consequently, it leads to a large PCM volume in the heat sink for a preferable effect. From Figure 10, it is noticed that with an increase in filling height, the performance score decreases. A decrease in foam height leads to a lesser amount of foams, and a longer melting period is observed. 10 mm filling height is higher performance score 1, and the least score 0 is spotted at 30 mm filling height. Whereas for 20 mm filling height, there is a slight improvement of the maximum score is noted.

When assessing the effects of porosity for filling height cases, there is a drop in performance with rising PPI. Except for 20 mm filling height, with 0.95 porosity at 20 PPI, all other cases follow the statement above. For all cases of foam height, 5 PPI with 0.95 porosity shows the best response. The reason behind this is with a decrease in PPI, less solid structure is introduced to PCM. Hence a reduced heat transfer is observed leading to extended melting.

The contours are plotted to have a better understanding of the temperature distribution and melt fraction curve. The heat sink with filling height of 20 mm at different pore size and pore density is considered in Figures 11 and 12 at time interval of 2000s.

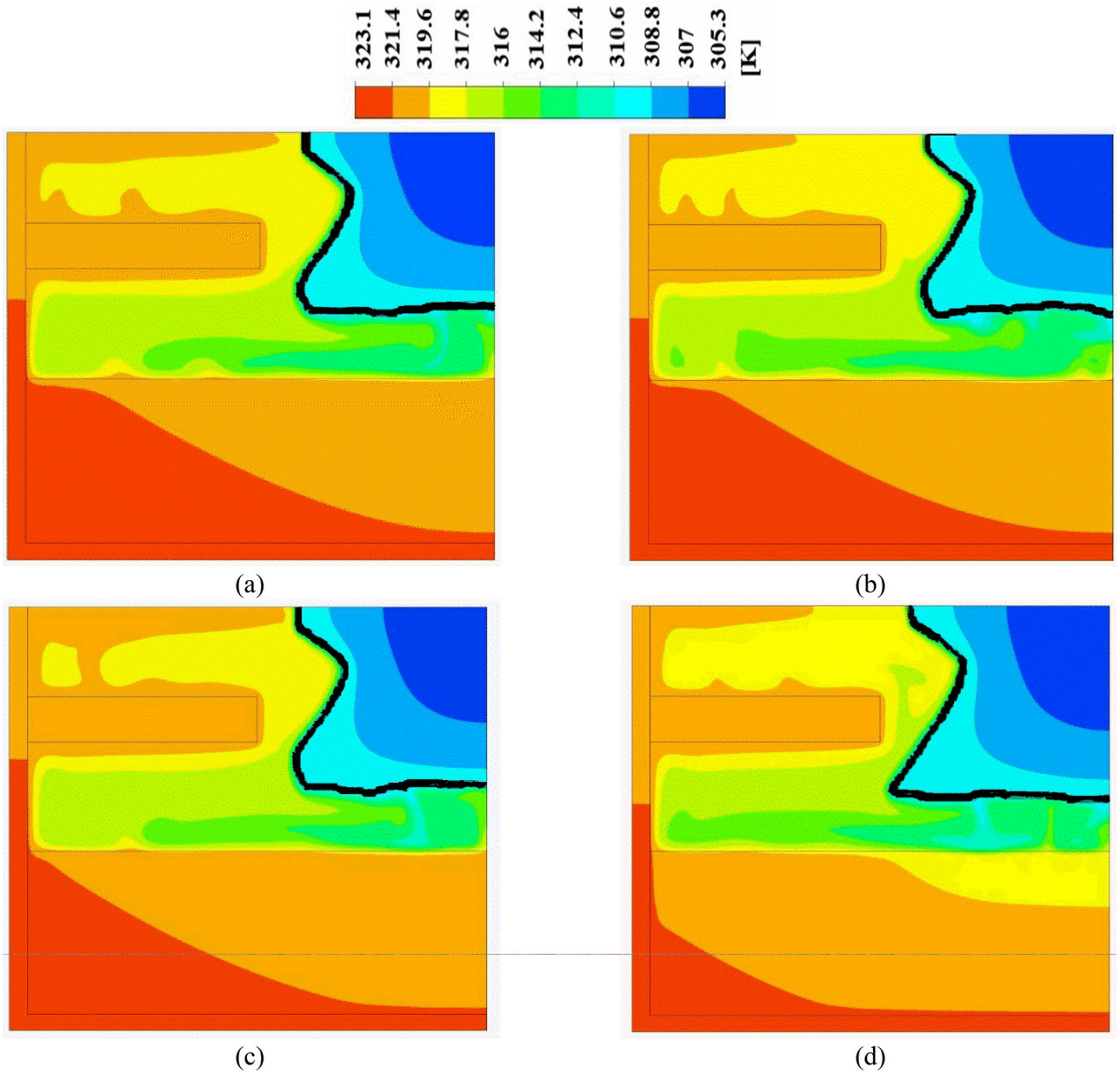


**Figure 11.** Contours of heat sink with filling height 20 mm at 25 PPI for different porosities (a) 0.8, (b) 0.85, (c) 0.9, and (d) 0.95.

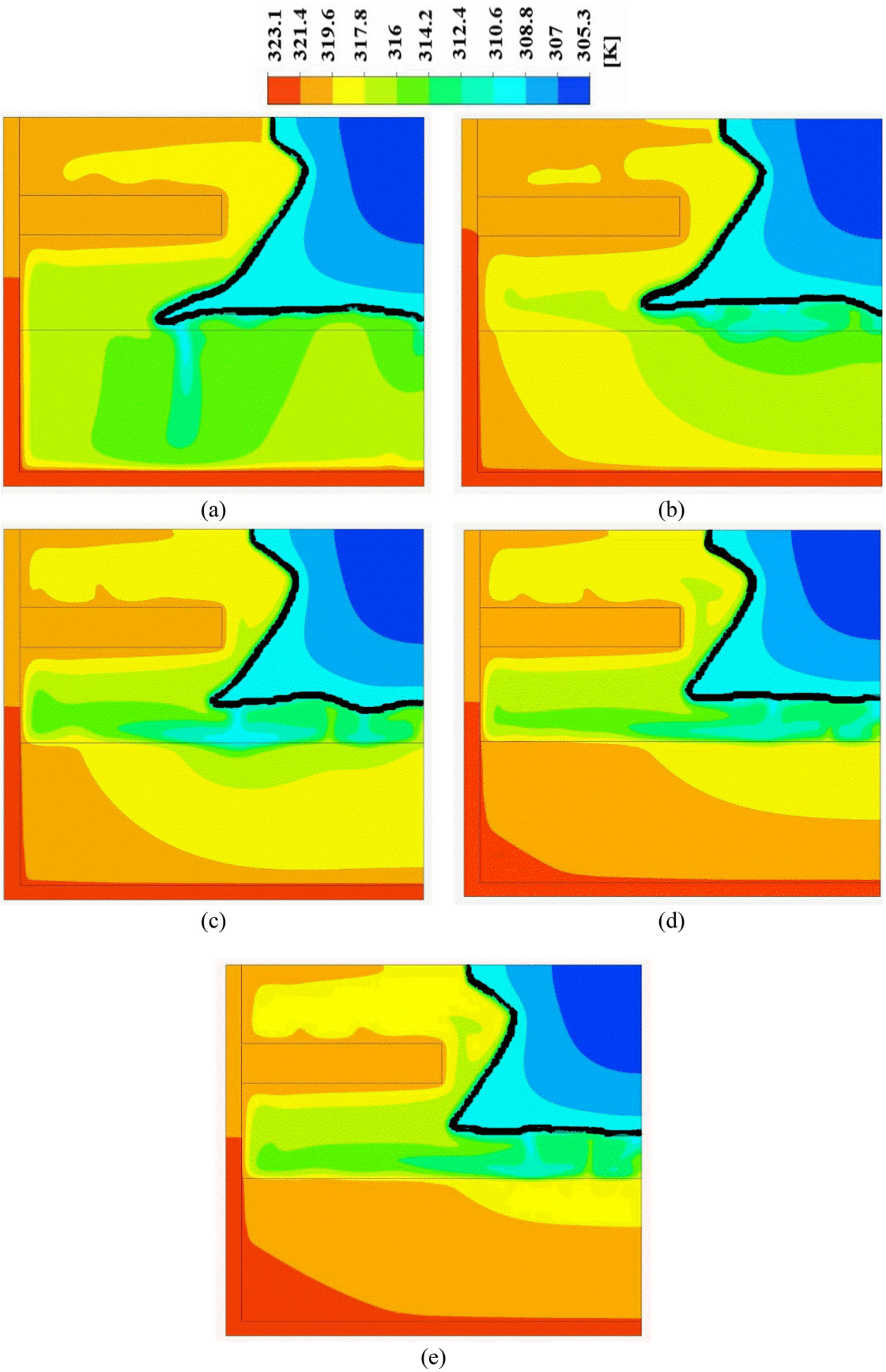


**Figure 12.** Contours of heat sink with filling height 20 mm at 0.95 porosity for different pore densities (a) 5 PPI, (b) 10 PPI, (c) 15 PPI, (d) 20 PPI, and (e) 25 PPI.

**Table 5.** Melting time in seconds for all cases.

| Filling height | 10 mm | | | | 20 mm | | | | 30 mm | | | |
|---|---|---|---|---|---|---|---|---|---|---|---|---|
| Porosity | | | | | | | | | | | | |
| PPI | *0.8* | *0.85* | *0.9* | *0.95* | *0.8* | *0.85* | *0.9* | *0.95* | *0.8* | *0.85* | *0.9* | *0.95* |
| ***5*** | 4153.2 | 4161.7 | 4230.4 | 4310.6 | 3490.8 | 3496 | 3551 | 3638.7 | 2835.4 | 2852.7 | 2886.6 | 3081.4 |
| ***10*** | 4121.3 | 4144.4 | 4203.2 | 4289.4 | 3479.6 | 3482.6 | 3527.9 | 3583.6 | 2812.5 | 2838.6 | 2860.7 | 3064.3 |
| ***15*** | 4095.2 | 4112 | 4181.8 | 4277.4 | 3471.2 | 3475.3 | 3513.7 | 3574.7 | 2784.7 | 2827.3 | 2836.2 | 3044.1 |
| ***20*** | 4067.6 | 4091.7 | 4121.8 | 4272.5 | 3417.1 | 3459.3 | 3497.3 | 3583.8 | 2772.3 | 2809.6 | 2827.1 | 3037.8 |
| ***25*** | 4042.7 | 4068.6 | 4108.1 | 4258 | 3348.4 | 3381.3 | 3423.1 | 3538.9 | 2762.9 | 2797.9 | 2811.5 | 3015.3 |

**Table 6.** Solidification time in seconds for all cases.

| Filling height | 10 mm | | | | 20 mm | | | | 30 mm | | | |
|---|---|---|---|---|---|---|---|---|---|---|---|---|
| Porosity | | | | | | | | | | | | |
| PPI | *0.8* | *0.85* | *0.9* | *0.95* | *0.8* | *0.85* | *0.9* | *0.95* | *0.8* | *0.85* | *0.9* | *0.95* |
| ***5*** | 44571 | 44618 | 44646 | 45257 | 34312 | 34398 | 34633 | 35189 | 22985 | 23002 | 23313 | 24290 |
| ***10*** | 43851 | 43939 | 44170 | 44591 | 33669 | 33742 | 33971 | 34431 | 22124 | 22312 | 22437 | 23276 |
| ***15*** | 43785 | 43874 | 44049 | 44294 | 33384 | 33470 | 33639 | 34053 | 21668 | 21800 | 22019 | 22769 |
| ***20*** | 43683 | 43786 | 43859 | 44166. | 33286 | 33327 | 33486 | 33873 | 21476 | 21597 | 21797 | 22504 |
| ***25*** | 43575 | 43685 | 43761 | 44063 | 33194 | 33244 | 33353 | 33726 | 21360 | 21446 | 21628 | 22293 |

**Table 7.** Ideal solutions for all criteria.

| Criteria | Melting/solidification time | Ideal positive/negative | Ideal solutions |
|---|---|---|---|
| Criteria-1 | $M_{max}$ | ideal positive | 0 |
| | | ideal negative | 0 |
| | $S_{min}$ | ideal positive | 0.08 |
| | | ideal negative | 0.168784354 |
| Criteria-2 | $M_{max}$ | ideal positive | 0.039381738 |
| | | ideal negative | 0.02505625 |
| | $S_{min}$ | ideal positive | 0.06 |
| | | ideal negative | 0.126588266 |
| Criteria-3 | $M_{max}$ | ideal positive | 0.078763476 |
| | | ideal negative | 0.0501125 |
| | $S_{min}$ | ideal positive | 0.04 |
| | | ideal negative | 0.084329177 |
| Criteria-4 | $M_{max}$ | ideal positive | 0.118145214 |
| | | ideal negative | 0.075168751 |
| | $S_{min}$ | ideal positive | 0.02 |
| | | ideal negative | 0.042196089 |
| Criteria-5 | $M_{max}$ | ideal positive | 0.157526952 |
| | | ideal negative | 0.100225001 |
| | $S_{min}$ | ideal positive | 0 |
| | | ideal negative | 0 |

The time interval of 2000s is selected, which shows a clear melt fraction and temperature plots. The melt fraction curve is displayed in black color, where liquid PCM is found below the curve and toward the heater surface and solid PCM is found above the curve. In Figure 11, the pore density is fixed at 25 PPI and porosity is varied and contours are obtained. It is clearly seen that with increasing porosity, the temperature distribution is found higher at low porosity. It is because for low porosity, the solid volume is higher and amount of PCM volume is less. Due to this, the completion of melting is found quicker at 0.8 porosity and slower at 0.95 porosity and vice versa for solidification. Next, in Figure 12, at 0.95 porosity different pore densities are varied and contours are plotted. A significant difference in temperature distribution and melt fraction curve is observed in Figure 12. As mentioned above, the solid volume influences the melting and solidification processes. With higher PPI, in both the cycles, the heat transfer performance is enhanced and completes the process at faster rate. The melting and solidification time for all the cases considered are listed in Tables 5 and 6. Also, the ideal positive/negative solutions value for all five criteria is given in Table 7.

## Conclusions

A two-dimensional numerical model for 60 cases was developed in ANSYS Fluent 19. The geometry with varying filling height and different pore structures was established in this study. The filling height was varied from 10 mm to 30 mm for a feasible heat sink strategy. The porosity ranging from 0.8-0.95 with increasing pore density from 5-25 PPI is altered for the study. A reliable algorithm of TOPSIS was used for multi-objective optimization. The two objective functions for the investigation were minimizing solidification time and maximizing melting time. Five criteria were selected based on the input weightage toward the objective function. On the basis of each criterion, performance scores were plotted for the required filling height, and the following observations are made.

- The evaluation of fin shape, fin placement and height are done initially. The rectangular fin shape with uniform thickness enhances the heat transfer with uniform temperature distribution within the enclosure. Considering effective outcome, the fins can be placed at 11 mm from the top surface with a height of 25 mm and a thickness of 5.6 mm.

- For criteria-1, the weightage is solely set toward the minimization of solidification, and no weightage is set for maximizing melting time. Hence, the higher filling heights yield accelerated solidification. Considering porous structure, the porosity of 0.8 with 25 PPI delivers the best performance for all cases of filling heights.
- In criteria-2, there is a one-quarter weightage toward maximizing the charging cycle and remaining toward minimizing discharging cycle. Similar to 1$^{st}$ criteria, filling height with a higher value also performs better. When it comes to porosity and PPI, for 10 mm and 30 mm filling height cases, 0.95 and 25 PPI provides higher scores. But for the 20 mm case, 0.8 porosity at 25 PPI has a preferable outcome.
- The weightage is shared equally between both the objective functions in criteria-3. Higher filling height dominates when the weightage is equal and more for minimizing solidification time with respect to maximizing melting time. Hence for the first three criteria, the filling height of 30 mm has a superior response compared to other filling heights. 25 PPI with 0.95 porosity has higher performance scores for all cases of filling heights.
- At criteria-4, the weightage is in favor of a prolonged melting period. When the weightage is altered, lesser filling height influences the system. Here for all filling heights, 0.95 porosity shows better results. Whereas accounting PPI, 25, 5, and 10 gives high scores for filling heights of 10, 20, and 30 mm, respectively.
- In the last criteria, opposite to criteria-1, the weightage is specified only for melting time maximization. As mentioned, when the weightage is applied for maximizing the charging cycle, 10 mm filling height dominates other cases. Assessing the porous structure, 5 PPI with 0.95 porosity metal foam generates prolonged melting.

This concludes that the porous matrix impacts the finned PCM-based systems at varying filling heights. Depending upon the weightage required, the filling height and porous physical characteristics can be selected. This description provides a deeper analysis of wide range of porous sizes and densities. Thus, these guidelines can be beneficial when partial filling can be employed with a fin on a PCM-based heat sink.

## Disclosure statement

No potential conflict of interest was reported by the authors.

## Notes on contributors

*Muthamil Selvan Nedumaran* is a research scholar in the Department of Mechanical Engineering at National Institute of Technology Karnataka, India. He graduated in Mechanical Engineering from CSI College of Engineering, The Nilgiris, Tamilnadu in 2014 and obtained his master's degree in Energy Engineering from PSG College of Engineering, Coimbatore, Tamilnadu in 2018. His research interests include numerical simulations, fluid flow and heat transfer in phase change materials, and experimental heat transfer. Currently carrying out research in the area of heat transfer through phase change materials under the supervision of Assistant Professor Nagarajan Gnanasekaran.

*Govindappa Trilok* is a research scholar in the Department of Mechanical Engineering at National Institute of Technology Karnataka, India. He graduated in Mechanical Engineering from University Visvesvaraya College of Engineering (UVCE), Bangalore, Karnataka in 2016 and obtained his master's degree in Thermal Science and Engineering from UVCE Bangalore, Karnataka in 2018. His research interests include computational fluid dynamics, optimization techniques and fluid flow and heat transfer through metal based porous media. Currently carrying out research in the area of flow and heat transfer behavior of metal based porous media such as metal foams and wire mesh porous structures under the supervision of Assistant Professor Nagarajan Gnanasekaran.

*Nagarajan Gnanasekaran* is an Assistant Professor in the Department of Mechanical Engineering at the National Institute of Technology Karnataka, India. He graduated in Mechanical Engineering (2002) from Bharathidasan University and obtained his Master of Engineering in Thermal Engineering (2006) from Government College of Technology, Coimbatore, and Ph.D. (2012) from Indian Institute of Technology Madras, Chennai. His research interests include computational inverse problems, bio-heat transfer, stochastic modeling techniques, experimental and numerical heat transfer, hybrid optimization, heat and fluid flow in porous media.

*Kamel Hooman* completed his Ph.D. at University of Queensland, for which he received a Dean's Award for Research Higher Degree Excellence and an Emerald Engineering Award (Outstanding Doctoral Research). He is a Professor of Heat Transformation Technology in the

Department of Process & Energy at the Delft University of Technology, Netherlands. His research focuses on both the fundamental and applied aspects of heat transformation and the conversion of renewable energy. He combines theoretical, numerical and experimental techniques with the aim of increasing the share of renewable energy and improving the efficiency of conventional systems. He is recognized worldwide for his work on heat exchangers and cooling towers which are essential technology for power generation and energy management. He has pioneered the use of metal foams in fuel cells, supercritical heat exchangers for geo/solar thermal power plants, and scaling of natural draft dry cooling towers. He is currently serving the International Journal of Heat and Mass Transfer, Journal of Porous Media, and Heat Transfer Engineering as an Associate Editor.

## References


[1] C. S. Miers and A. Marconnet, "Experimental investigation of composite phase change material heat sinks for enhanced passive thermal management," *J. Heat Transfer*, vol. 143, no. 1, pp. 013001, Jan. 2021. DOI: 10.1115/1.4048620.

[2] S. K. Saha and P. Dutta, "Role of melt convection on optimization of pcm-based heat sink under cyclic heat load," *Heat Transf. Eng.*, vol. 34, no. 11-12, pp. 950–958, 2013. DOI: 10.1080/01457632.2012.753574.

[3] R. D. C. Oliveski, F. Becker, L. A. O. Rocha, C. Biserni and G. E. S. Eberhardt, "Design of fin structures for phase change material (PCM) melting process in rectangular cavities," *J. Energy Storage*, vol. 35, pp. 102337, Mar. 2021. DOI: 10.1016/j.est.2021.102337.

[4] V. Palomba, et al., "Latent thermal storage for solar cooling applications: materials characterization and numerical optimization of finned storage configurations," *Heat Transfer Eng.g*, vol. 40, no. 12, pp. 1033–1048, 2019. DOI: 10.1080/01457632.2018.1451236.

[5] R. Baby and C. Balaji, "Experimental investigations on phase change material based finned heat sinks for electronic equipment cooling," *Int. J. Heat Mass Transfer*, vol. 55, no. 5-6, pp. 1642–1649, Feb. 2012. DOI: 10.1016/j.ijheatmasstransfer.2011.11.020.

[6] C. Zhao, et al., "Simulations of melting performance enhancement for a PCM embedded in metal periodic structures," *Int. J. Heat Mass Transfer*, vol. 168, pp. 120853, Apr. 2021. DOI: 10.1016/j.ijheatmasstransfer.2020.120853.

[7] R. Baby and C. Balaji, "Experimental investigations on thermal performance enhancement and effect of orientation on porous matrix filled PCM based heat sink," *Int. Commun. Heat Mass Transfer*, vol. 46, pp. 27–30, Aug. 2013. DOI: 10.1016/j.icheatmasstransfer.2013.05.018.

[8] B. Buonomo, D. Ercole, O. Manca and S. Nardini, "Numerical analysis on a latent thermal energy storage system with phase change materials and aluminum foam," *Heat Transfer Eng.*, vol. 41, no. 12, pp. 1075–1084, 2020. DOI: 10.1080/01457632.2019.1600875.

[9] S. Mancin, A. Diani, L. Doretti, K. Hooman and L. Rossetto, "Experimental analysis of phase change phenomenon of paraffin waxes embedded in copper foams," *Int. J. Therm. Sci.*, vol. 90, pp. 79–89, Apr. 2015. DOI: 10.1016/j.ijthermalsci.2014.11.023.

[10] H. Xu, Y. Wang and X. Han, "Analytical considerations of thermal storage and interface evolution of a PCM with/without porous media," *HFF*, vol. 30, no. 1, pp. 373–400, Jan. 2019. DOI: 10.1108/HFF-02-2019-0094.

[11] M. R. Assari, H. Basirat Tabrizi, M. Shafiee and Y. Cheshmeh Khavar, "Experimental performance of desalination system using solar concentrator, nanofluid, and preheater tube accompanying phase change material," *Iran. J. Sci. Technol. Trans. Mech. Eng.*, vol. 45, no. 4, pp. 1033–1044, 2021. DOI: 10.1007/s40997-020-00383-4.

[12] L. Colla, et al., "Nano-phase change materials for electronics cooling applications," *J. Heat Transfer*, vol. 139, no. 5, pp. 052406, May 2017. DOI: 10.1115/1.4036017.

[13] H. Faraji, M. Faraji and M. El Alami, "Numerical study of the transient melting of nano-enhanced phase change material," *Heat Transfer Eng.*, vol. 42, no. 2, pp. 120–139, 2021. DOI: 10.1080/01457632.2019.1692496.

[14] M. Abdollahzadeh and M. Esmaeilpour, "Enhancement of phase change material (PCM) based latent heat storage, system with nano fluid and wavy surface," *Int. J. Heat Mass Transfer*, vol. 80, pp. 376–385, Jan. 2015. DOI: 10.1016/j.ijheatmasstransfer.2014.09.007.

[15] A. K. Gupta, G. Mishra and S. Singh, "Numerical study of MWCNT enhanced PCM melting through a heated undulated wall in the latent heat storage unit," *Therm. Sci. Eng. Prog.*, vol. 27, pp. 101172, Jan. 2022. DOI: 10.1016/j.tsep.2021.101172.

[16] A. Ghanbarpour, et al., "Evaluation of heat sink performance using PCM and vapor chamber/heat pipe," *Renewable Energy*, vol. 163, pp. 698–719, Jan. 2021. DOI: 10.1016/j.renene.2020.08.154.

[17] G. K. Marri and C. Balaji, "Experimental and numerical investigations on a phase change material based heat sink with symbiotically joined heat pipe," *Heat Transfer Eng.*, vol. 42, no. 1, pp. 23–40, 2021. DOI: 10.1080/01457632.2019.1685241.

[18] H. Behi, et al., "PCM assisted heat pipe cooling system for the thermal management of an LTO cell for high-current profiles," *Case Stud. Therm. Eng.*, vol. 25, pp. 100920, Jun. 2021. DOI: 10.1016/j.csite.2021.100920.

[19] A. N. Desai, H. Shah and V. K. Singh, "Novel inverted fin configurations for enhancing the thermal performance of PCM based thermal control unit: a numerical study," *Appl. Therm. Eng.*, vol. 195, pp. 117155, Aug. 2021. DOI: 10.1016/j.applthermaleng.2021.117155.

[20] X. Luo, et al., "Numerical study on enhanced melting heat transfer of PCM by the combined fractal fins," *J. Energy Storage*, vol. 45, pp. 103780, Jan. 2022. DOI: 10.1016/j.est.2021.103780.

[21] M. R. Singh and A. Giri, "A comparison of the performance of constant and dual height pin fins in

phase change material cooling technique," *J. Therm. Sci. Eng. Appl.*, vol. 13, no. 4, pp. 041027, Mar. 2021. DOI: 10.1115/1.4048665.

[22] Z. Chen, D. Gao and J. Shi, "Experimental and numerical study on melting of phase change materials in metal foams at pore scale," *Int. J. Heat Mass Transfer*, vol. 72, pp. 646–655, May 2014. DOI: 10.1016/j.ijheatmasstransfer.2014.01.003.

[23] S. Wang, et al., "Experimental study on the thermal performance of PCMs based heat sink using higher alcohol/graphite foam," *Appl. Therm. Eng.*, vol. 198, pp. 117452, Nov. 2021. DOI: 10.1016/j.applthermaleng.2021.117452.

[24] C. Zhao, et al., "Phase change behavior study of PCM tanks partially filled with graphite foam," *Appl. Therm. Eng.*, vol. 196, pp. 117313, Sep. 2021. DOI: 10.1016/j.applthermaleng.2021.117313.

[25] J. M. Mahdi, H. I. Mohammed, E. T. Hashim, P. Talebizadehsardari and E. C. Nsofor, "Solidification enhancement with multiple PCMs, cascaded metal foam and nanoparticles in the shell-and-tube energy storage system," *Appl. Energy*, vol. 257, pp. 113993, Jan. 2020. DOI: 10.1016/j.apenergy.2019.113993.

[26] H. J. Xu and C. Y. Zhao, "Thermal performance of cascaded thermal storage with phase-change materials (PCMs). Part I: steady cases," *Int. J. Heat Mass Transfer*, vol. 106, pp. 932–944, Mar. 2017. DOI: 10.1016/j.ijheatmasstransfer.2016.10.054.

[27] J. M. Mahdi and E. C. Nsofor, "Solidification enhancement of PCM in a triplex-tube thermal energy storage system with nanoparticles and fins," *Appl. Energy*, vol. 211, pp. 975–986, Feb. 2018. DOI: 10.1016/j.apenergy.2017.11.082.

[28] H. A. Refaey, M. H. Wahba, H. E. Abdelrahman, M. Moawad and N. S. Berbish, "Experimental Study on the Performance Enhancement of the Photovoltaic Cells by Using Various Nano-Enhanced PCMs," *J. Inst. Eng. India Ser. C*, vol. 102, no. 2, pp. 553–562, Jan. 2021. DOI: 10.1007/s40032-020-00655-7.

[29] Z. Khan and Z. A. Khan, "Performance evaluation of coupled thermal enhancement through novel wire-wound fins design and graphene nano- platelets in shell-and-tube latent heat storage system," *Energies*, vol. 14, no. 13, pp. 3743, Jun. 2021. DOI: 10.3390/en14133743.

[30] M. H. S. Abandani and D. D. Ganji, "Melting effect in triplex-tube thermal energy storage system using multiple PCMs-porous metal foam combination," *J. Energy Storage*, vol. 43, pp. 103154, Nov. 2021. DOI: 10.1016/j.est.2021.103154.

[31] Q. Ren, F. Meng and P. Guo, "A comparative study of PCM melting process in a heat pipe-assisted LHTES unit enhanced with nanoparticles and metal foams by immersed boundary-lattice Boltzmann method at pore-scale," *Int. J. Heat Mass Transfer*, vol. 121, pp. 1214–1228, Jun. 2018. DOI: 10.1016/j.ijheatmasstransfer.2018.01.046.

[32] A. Nagose, A. Somani, A. Shrot and A. Narasimhan, "Genetic algorithm based optimization of PCM based heat sinks and effect of heat sink parameters on operational time," *J. Heat Transfer*, vol. 130, no. 1, pp. 011401, Jan. 2008. DOI: 10.1115/1.2780182.

[33] A. Pizzolato, A. Sharma, K. Maute, A. Sciacovelli and V. Verda, "Design of effective fins for fast PCM melting and solidification in shell-and-tube latent heat thermal energy storage through topology optimization," *Appl. Energy*, vol. 208, pp. 210–227, Dec. 2017. DOI: 10.1016/j.apenergy.2017.10.050.

[34] P. P. Levin, A. Shitzer and G. Hetsroni, "Numerical optimization of a PCM-based heat sink with internal fins," *Int. J. Heat Mass Transfer*, vol. 61, pp. 638–645, Jun. 2013. DOI: 10.1016/j.ijheatmasstransfer.2013.01.056.

[35] J. Xie, H. M. Lee and J. Xiang, "Numerical study of thermally optimized metal structures in a Phase Change Material (PCM) enclosure," *Appl. Therm. Eng.*, vol. 148, pp. 825–837, Feb. 2019. DOI: 10.1016/j.applthermaleng.2018.11.111.

[36] M. Augspurger, K. K. Choi and H. S. Udaykumar, "Optimizing fin design for a PCM-based thermal storage device using dynamic Kriging," *Int. J. Heat Mass Transfer*, vol. 121, pp. 290–308, Jun. 2018. DOI: 10.1016/j.ijheatmasstransfer.2017.12.143.

[37] A. Singh, S. Rangarajan, L. Choobineh and B. Sammakia, "Figure of merit-based optimization approach of phase change material-based composites for portable electronics using simplified model," *J. Electron Package*, vol. 144, no. 2, pp. 021104, Jun. 2022. DOI: 10.1115/1.4052074.

[38] M. S. Nedumaran and N. Gnanasekaran, "Comprehensive analysis of hybrid heat sinks with phase change materials for both charging and discharging cycles," *Heat Transfer Eng.*, vol. 44, no. 4, pp. 334–352, Apr. 2023. DOI: 10.1080/01457632.2022.2059216.

[39] C. Ji, et al., "Non-uniform heat transfer suppression to enhance PCM melting by angled fins," *Appl. Therm. Eng.*, vol. 129, pp. 269–279, Jan. 2018. DOI: 10.1016/j.applthermaleng.2017.10.030.

[40] C. Ji, et al., "Simulation on PCM melting enhancement with double-fin length arrangements in a rectangular enclosure induced by natural convection," *Int. J. Heat Mass Transfer*, vol. 127, pp. 255–265, Dec. 2018. DOI: 10.1016/j.ijheatmasstransfer.2018.07.118.

[41] ANSYS FLUENT., *ANSYS Fluent 12.0 User's Guide*. Canonsburg, PA: Ansys Inc, 2009. http://scholar.google.com/scholar?hl=en&btnG=Search&q=intitle:ANSYS+FLUENT+User+'+s+Guide#1.

[42] V. V. Calmidi and R. L. Mahajan, "Forced convection in high porosity metal foams," *J. Heat Transfer*, vol. 122, no. 3, pp. 557–565, Aug. 2000. DOI: 10.1115/1.1287793.

[43] V. V. Calmidi, "Transport phenomena in high porosity fibrous metal foams," Ph.D. thesis, University of Colorado, Boulder, CO, 1998. https://www.semanticscholar.org/paper/Transport-phenomena-in-high-porosity-fibrous-metal-Calmidi/53d17b0c79c986425deb49b32bb0ab22fcdd155a#paper-header.

[44] K. Boomsma and D. Poulikakos, "On the effective thermal conductivity of a three-dimensionally structured fluid-saturated metal foam," *Int. J. Heat Mass Transfer*, vol. 44, no. 4, pp. 827–836, Feb. 2001. DOI: 10.1016/S0017-9310(00)00123-X.

[45] W. Lu, T. Zhang and M. Yang, "Analytical solution of forced convective heat transfer in parallel-plate channel partially filled with metallic foams," *Int. J. Heat Mass Transfer*, vol. 100, pp. 718–727, Sep. 2016. DOI: 10.1016/j.ijheatmasstransfer.2016.04.047.

[46] H. Zheng, C. Wang, Q. Liu, Z. Tian and X. Fan, "Thermal performance of copper foam/paraffin composite phase change material," *Energy Convers Manage*, vol. 157, pp. 372–381, Feb. 2018. DOI: 10.1016/j.enconman.2017.12.023.

[47] P. H. Jadhav, N. Gnanasekaran, D. A. Perumal and M. Mobedi, "Performance evaluation of partially filled high porosity metal foam configurations in a pipe," *Appl. Therm. Eng.*, vol. 194, pp. 117081, Jul. 2021. DOI: 10.1016/j.applthermaleng.2021.117081.

[48] G. Trilok and N. Gnanasekaran, "Numerical study on maximizing heat transfer and minimizing flow resistance behavior of metal foams owing to their structural properties," *Int. J. Therm. Sci.*, vol. 159, pp. 106617, Jan. 2021. DOI: 10.1016/j.ijthermalsci.2020.106617.

[49] Z.-Q. Zhu, Y.-K. Huang, N. Hu, Y. Zeng and L.-W. Fan, "Transient performance of a PCM-based heat sink with a partially filled metal foam: effects of the filling height ratio," *Appl. Therm. Eng.*, vol. 128, pp. 966–972, Jan. 2018. DOI: 10.1016/j.applthermaleng.2017.09.047.